SOLUTION MINING RESEARCH INSTITUTE

679 Plank Road
Clifton Park, NY 12065, USA

Telephone: +1 518-579-6587
www.solutionmining.org

Technical Conference Paper

1965 – 2025

Evaluation of Downhole Completion Technology and Material Samples Following a Successful Underground Hydrogen Storage Demonstration in the Netherlands

Patrick Roordink[1], Fraser Murray[2], Bert De Vries[2], Darrell Adkins[2], Arpana Verma[2], Sandeep Thatathil[2], Shashwat Shuckla[2]

Nederlandse Gasunie N.V.[1], Halliburton[2]

SMRI Spring 2025 Technical Conference
27-29 April 2025
Wilhelmshaven, Germany

Solution Mining Research Institute Spring 2025 Conference

Wilhelmshaven, Germany, 27-29 April 2025

Evaluation of Downhole Completion Technology and Material Samples Following a Successful Underground Hydrogen Storage Demonstration in the Netherlands

Patrick Roordink[1], Fraser Murray[2], Bert De Vries[2], Darrell Adkins[2], Arpana Verma[2], Sandeep Thatathil[2], Shashwat Shuckla[2]

Nederlandse Gasunie N.V.[1], Halliburton[2]

Abstract

A project was conducted in the Netherlands to demonstrate safe storage of hydrogen in an underground salt cavern. This pilot represents one of the first global fast-cyclic energy system demonstrations to prove the feasibility of pure hydrogen storage using methods analogous to underground natural gas storage. Downhole completion technology was supplied including a 9 5/8-in. SP™ tubing retrievable safety valve (TRSV), 13 3/8-in. X-Trieve™ HC production packer, OTIS® RPT® No-Go landing nipples, and a material test sub. The well was exposed to hydrogen for a period of 11 months with surface pressure and temperature up to 200 bar (2,900 psi) and 42°C (149°F). The production packer demonstrated annular integrity throughout the demonstration project and even under well cycling. The safety valve was manually cycled more than 75 times with zero leakage across the high-performance rod piston seals or body connections. The safety valve was also inflow tested seven times and demonstrated performance far exceeding current oil and gas (O&G) acceptance criteria.

Following conclusion of demonstration activities, the well was de-completed and the downhole technologies, including safety valve, production packer and material test sub were retrieved for further evaluation. Initial inspection and testing activities were performed at a nearby field location and within hours of recovery from the well. The technologies were then returned to the Halliburton Completion Tools Centre of Excellence in Singapore for a more rigorous study. There, the safety valve successfully underwent a suite of testing, largely replicating that performed on a newly manufactured valve. Both the safety valve and production packer underwent post-test inspection and disassembly with observations driving new design and material-based recommendations.

The material test sub included a total of 64 pre-stressed metallic material samples (eight of which were supplied by the operator) including low-alloy steel, stainless steel, Ni- and Co-base superalloy, weldments, and coatings, which were subjected to stresses within a range of 67 to 90% yield strength. Additionally, 150 non-metallic samples including HNBR, FKM, FEPM, FFKM, PTFE, and PEEK were included. All material samples were returned to the Halliburton Material Science Centre of Excellence in Singapore for further evaluation. Metallic material samples were scrutinized through visual, LPI, laser scanning and X-ray CT methods, while non-metallic specimens underwent visual and X-ray CT with mechanical and analytical property change evaluation through FTIR (Fourier Transform Infrared Spectroscopy), DSC (Differential Scanning Calorimetry) and TGA techniques (Thermogravimetric Analysis). The outcome of this effort defined a path for future material studies which are currently under execution phase.

This paper/presentation will focus on the operational performance, post-test evaluation and recommendations related to the completion tools and material samples included in this demonstration project.

Key words: Hydrogen, Gas storage, Materials, Metallic, Polymer, Elastomer, Plastic

1. Introduction

Large-scale hydrogen storage plays a critical role in the fast-growing hydrogen economy. As such, operators continue to drill new wells or convert depleted wells and existing caverns for hydrogen storage applications. On the material science front, understanding the compatibility of various metallic and non-metallic materials with hydrogen gas during long-term exposure is crucial to development of hydrogen storage well components. The Halliburton Material Science team is aggressively working to evaluate material performance in hydrogen environments. As part of this initiative, Halliburton collaborated with Gasunie, Netherlands, to perform real-time evaluation of different materials in a hydrogen storage pilot well. In addition to the standard tools, the Halliburton team designed and developed a special test sub for material exposure to the well environment. The test sub was attached to the completion equipment, which included a 9 5/8-in. SP™ tubing-retrievable safety valve (TRSV), 13 3/8-in. × 9 5/8-in. X-Trieve™ HC AHC packer, and 8.313- and 8.250-in. RPT® landing nipples. The well was operational approximately one year from January 31, 2022, to January 22, 2023, with hydrogen stored until December 6, 2022. Once the hydrogen was removed from the well, fully saturated brine was pumped into the well from December 6, 2022, through January 22, 2023.

Completion equipment along with the material test sub were retrieved from the well January 22, 2023, test samples were removed, and initial inspection of the samples and tools was performed at the Halliburton base in Emmen, Netherlands. All samples were observed to be in good condition with no surface or RGD defects. The samples were then sent to the Material Science Lab in Singapore for further investigation and to study the effects of hydrogen exposure.

This report consolidates the evaluation of metallic and non-metallic samples exposed to a hydrogen environment in the Gasunie test well in The Netherlands. The effects of hydrogen on common oil and gas material selections, including low-alloy steel, martensitic stainless steel and superalloy, elastomers, and engineered plastic are summarized.

2. Project Overview

The Netherlands aims for zero CO_2 emissions by 2050, with sustainable hydrogen playing a key role. There is a need for large-scale underground storage of hydrogen because supply and demand of hydrogen are not constant. Within the HyStock project, N.V. Nederlandse Gasunie (Gasunie) performed a pilot demonstration project for the storage of hydrogen on well ZW A8A at their existing gas storage field Aardgasbuffer Zuidwending to show the technical feasibility of these operations. The long-term objective is the creation of caverns for hydrogen storage. This has already been realized in various other areas (3 x US, 1 x UK, 1 x Germany) this however based on different legal requirements and Standards. In other European countries (Germany, France), pilot projects are being carried out to show the technical feasibility.

The aim of the demonstration phase was to investigate the influences of hydrogen on well materials and to demonstrate that hydrogen storage in salt caverns is conform with Dutch safety standards and regulations. This pilot demonstration project can be divided into two separate stages:

1. Check of the well tightness related to hydrogen.

2. Check of suitability of involved equipment, services, and operational setup for hydrogen applications.

In the first stage, the project included the assessment of the well's integrity using a combined mechanical integrity testing (MIT) approach. In a two-step procedure, the verification of the borehole's gas tightness was proven by a MIT with nitrogen (N_2) and hydrogen (H_2) as test fluids.

Subsequently in the second stage, the execution of a systematic hydrogen storage test run over a period of several months was realized to check the "H_2-readiness" of equipment (the focus of this paper), involved services and the operational setup. Experts have been involved in analysing the

results of the demonstration and close consultation was held with regulator State Supervision of Mines. The preparations of the project started in 2019, and last activities were completed in 2023.

3. Pilot Well Completion Technology Performance and Evaluation

A pilot project was conducted in the Netherlands to demonstrate that pure hydrogen can be safely stored in an underground salt cavern. A single well was drilled and cased to a depth of 1290m and a completion comprising of a 9 5/8-in injection/production string, 9 5/8-in. tubing retrievable surface controlled subsurface safety valve, 13 3/8-in. X 9 5/8-in. hydraulic set retrievable production packer, two top no-go landing nipples and a material test sub was installed. A simple completion schematic is provided in figure 1. The well was not leached into a full-size storage cavern to maintain low hydrogen handling volumes. The material test sub is a patented design and was specifically developed for this pilot project. The sub enabled an array of 64 pre-stressed metallic and 150 non-metallic material samples to be conveyed into the well for long-term hydrogen exposure per figure 2. Further details around the materials and results are discussed later in this paper.

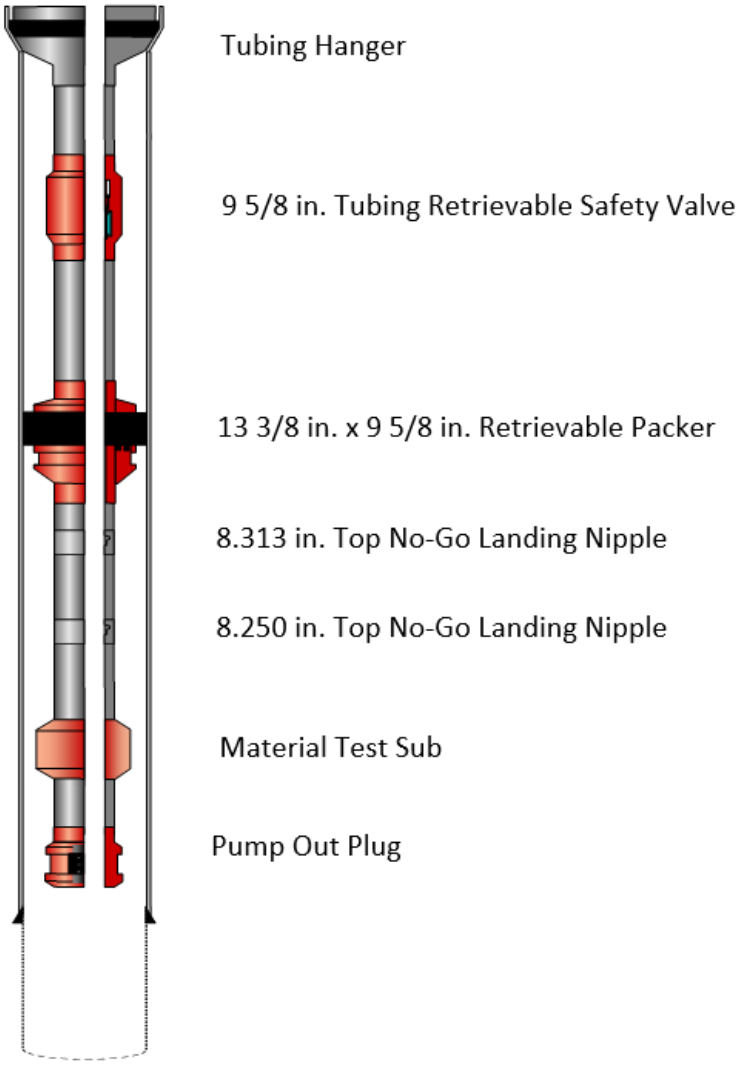

Figure 1: A8 Well Completion Design

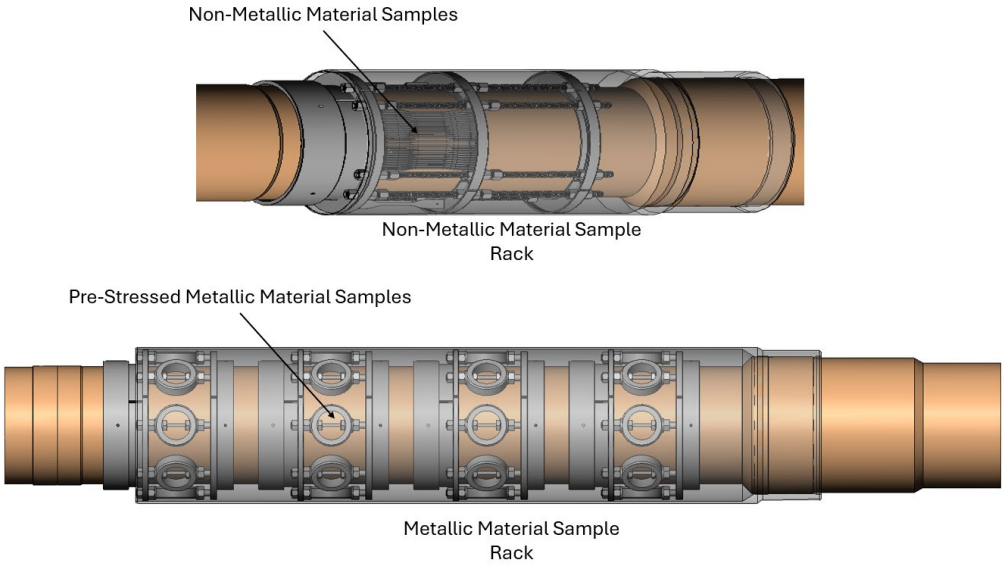

Figure 2: Material Test Sub Design

The subsurface safety valve and production packer are safety critical devices. Although both selected technologies have successful track record in oil and gas, along with underground methane storage, no previous hydrogen storage experience existed placing significant focus on their performance during this pilot project. An introduction to both technologies is provided in the coming sections.

The production packer is conveyed into the well as part of the injection/production string with the design including critical features including slips, element, body lock ring, a hydraulic setting feature and a cut to release retrieval feature per figure 3. The packer is run in the well to the intended depth and is set through the application of tubing pressure against a plug at the bottom of the completion. During the setting sequence the packer slips, and element are deployed to provide anchoring and sealing capability while the body lock ring retains the packer in the set position once the setting pressure is relieved. This anchoring and sealing capability must remain throughout life of well to control hydrogen placement and prevent leakage into the upper A-annulus. The packer can be released by performing a through thickness cut at a defined location on the internal mandrel enabling recovery if the entire completion string from the well.

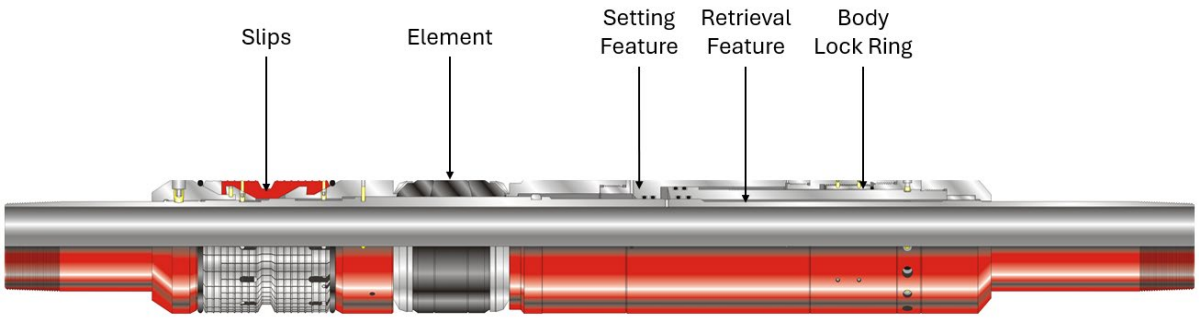

Figure 3: Production Packer Main Features

The subsurface safety valve is also conveyed into the well with the injection/production string. The design includes critical features including a flapper and seat, power spring, opening prong and hydraulic actuator per figure 4. A 1/4 in. hydraulic control line is attached to a port at the top of the safety valve enabling pressure application to the hydraulic actuator. When sufficient pressure is applied to the actuator it pushes the opening prong downward, compressing the power spring and opening the flapper to enable injection or production from the well. The open configure is demonstrated in figure 4. When pressure is relieved from the control line, and subsequently the hydraulic actuator, the safety

valve closes to significantly restrict the flow back of fluid from the well to the surface. This would normally occur during a loss of containment scenario to minimize the impact of fluid leakage. These valves are considered ‘fail safe close’ as even with the loss of control line integrity the valve will ‘fail’ in the closed position.

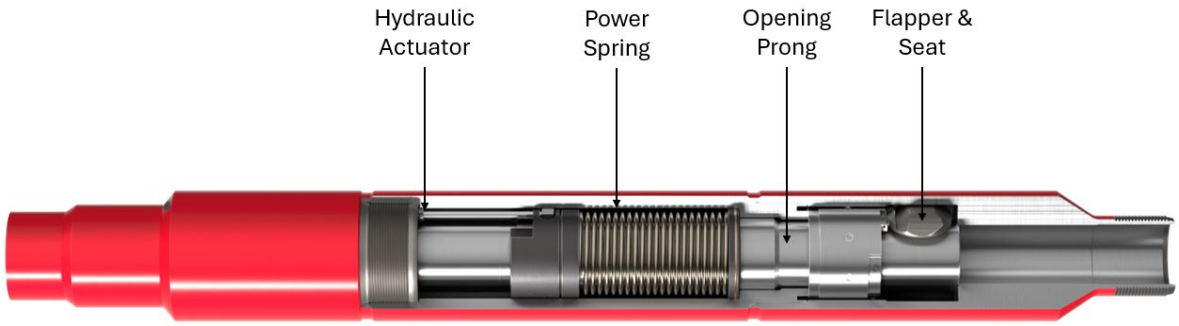

Figure 4: Subsurface Safety Valve Main Features

Safety valves and production packers used by the oil and gas industry can be qualified per existing industry standards, most notably API 14A for safety valves and API 11D1 for production packers. The infancy of the hydrogen storage industry means that neither of these standards offer specific guidance for hydrogen storage thereby leaving the industry short of a defined method to evaluate environmental and operational functionality for such applications. It is possible that future revision of the standards will include specific guidance for hydrogen storage but in the meantime and certainly for this pilot project technology providers and well operators need to identify an appropriate approach for each application. In the case of this pilot a decision was made to evaluate the technology performance during the demonstration project. This was acceptable on the basis that hydrogen volumes were low and the operational timeline was relatively short. For operators advancing directly to full scale development projects where risks and consequences are higher, then a desire might exist to perform additional testing ahead of operations like that described by Busollo et al, 2024.

The completion was installed in January 2022 while the well was filled with a brine medium. The production packer was successfully set and tested along with the remainder of the 9 5/8-in string confirming integrity ahead of introducing hydrogen. The brine was removed from the well and replaced with hydrogen which would remain for a period of approximately 11 months. Surface pressures and temperatures of between 0 to 200 bar (0 to 2900 psi) and -10 to 44°C (14°F to 111°F) were recorded during the hydrogen exposure period. The A-annulus surface pressure was continually monitored without abnormal observation verifying production packer integrity throughout. Additionally, two site visits were made by Halliburton to conduct additional testing on the subsurface safety valve. During this in-situ test program a total of 75 operating cycles were performed to actuate the valve between fully open and fully closed positions. The valve was observed to operate without hesitation or anomaly. Throughout these cycles the operating control line was opened to the atmosphere allowing the rod piston seal assembly to be inflow tested against the pressure within the injection/production string. The bubble detection apparatus recorded zero leakage throughout all hydraulic actuator inflow tests. Additionally, a total of seven inflow tests were performed across the safety valve flapper by firstly closing the safety valve and venting the pressure in the injection/production string above it. All inflow test results were far superior to the expectations of API 14B which recommends a maximum leakage rate of 15 scf/min for oil and gas applications. In summary, all completion technology was found to perform without concern during the full hydrogen exposure period.

Upon conclusion of the demonstration project hydrogen exposure period the completion was recovered providing a unique opportunity to physically examine the downhole technologies. The tools were promptly returned to the Halliburton operational base in Emmen, Netherlands, where all technologies were found to be in good visual condition. The safety valve underwent baseline performance tests,

including functionally operating the valve open and closed with and without bore pressure, along with inflow testing the flapper. These tests identified zero operational or sealing performance issues. The production packer was observed to have set and released as expected with a through-thickness cut identified within the mandrel cut zone. The material test sub was observed intact with all material samples retained. These material samples were removed from the sub and along with the production packer and subsurface safety valve shipped back to the Halliburton Centre of Excellence in Singapore.

The subsurface safety valve underwent a thorough test program throughout which operation and sealing capability were evaluated using a gas test medium. All leakage tests met the manufactures requirements for newly manufactured valves which are already 5 times stricter than those imposed by API 14A annex C. It was then disassembled and inspected, with the presence of debris deposits and corrosion, predominately on the low-alloy steel components, being the only notable observations. The production packer was inspected and disassembled. Beyond similar corrosion of low-allow steel components, an improvement opportunity was identified in removing the connection between upper and lower mandrels. This change has been implemented in future design revisions.

4. Material Science Methods

A specially designed test sub was used to introduce and expose the samples to test well. The well was filled with brine for 15 days prior to and after hydrogen exposure. Pure hydrogen with a purity of 99.99% was pumped into the well and the hydrogen pressure was maintained in the range of 100 to 200 bar (1450 to 2900 psi). No other chemical or gas injected into the well throughout the exposure period. Down hole well temperature was around 44°C (111°F) and hydrogen bleed off was performed at a slow rate of 20 bar/30 min. Table 1 provides well condition details.

Parameters	**Observations**
Bottomhole pressure	Wellhead + 2 bar
Bottomhole temperature	Approximately 44°C (111°F)
Hydrogen exposure period	11 months + 6 days
Purity of hydrogen/composition	99.99%
Hydrogen pressure (minimum/maximum)	100 to 200 bar (1450 to 2900 psi)
Hydrogen bleed rate	10 psi/min (0.689 bar/min)
Presence of H_2S in the well	Nil
Brine composition	Fully saturated NaCl brine 1.200 kg/cm^3
Brine exposure period	15 days before hydrogen exposure and 15 days after exposure
Brine pH	Not known
Any other treatment (acid exposure)	No other gas or chemical exposure

Table 1: Test Well Conditions

5. Material Selection

Samples from selected low-alloy steel grades, Ni-base superalloy, and weldments and coatings were exposed to the well for evaluation. Cylindrical subsize tensile test coupons were machined as per *ASTM A370*. These specimens were preloaded to subject them to a predefined constant tensile stress during hydrogen exposure. The preloading was done to stress at a range of 67 to 90% YS in a high-pressure hydrogen environment Table 2 lists the bulk metallic materials selected and exposed to the hydrogen environment.

Material	Load
4130M 110MY	67 & 90 (% Actual YS)
4130M 125MY	67 & 90 (% Actual YS)
4140 80MY	67 & 90 (% Actual YS)
4140 125MY	67 & 90 (% Actual YS)
925 110MY	67 & 90 (% Actual YS)
718 125MY	67 & 90 (% Actual YS)
X-750 180 MIN UTS	50 (% Actual UTS)
R30003 230 MIN UTS	50 (% Actual UTS)
R30035 230 MIN UTS	67 & 90 (% Actual YS)
410SS 80MY	67 & 90 (% Actual YS)
420M 80MY	67 & 90 (% Actual YS)

Table 2: Metallic Materials Selected for Hydrogen Exposure

Even though samples of weldments and coatings were also exposed to the well condition; their analysis was limited to a preliminary NDT.

Metallic samples loaded on the test sub is illustrated in Figure 5.

Figure 5: Metallic Sample Loading Arrangement on Test Sub

Commonly used elastomeric materials: Hydrogenated nitrile rubber (HNBR), Fluorocarbon rubber (FKM), Tetrafluoroethylene Propylene Monomer (FEPM), and Perfluoro elastomer (FFKM) were considered for evaluation. Nitrile rubber (NBR) is not included in the scope of study due to its poor resistance to impurities like H_2S. Thermoplastic materials – Polytetrafluoroethylene (PTFE) and Polyether ether ketone (PEEK) were considered during evaluation. Following the gas exposure practice, all elastomer materials selected were RGD-resistant materials in accordance with Halliburton specifications. Table 3 lists the non-metallic material selected and exposed to the hydrogen environment.

Material	Load
HNBR	No preload
FKM	No preload
FEPM AFLAS®	No preload
FFKM	No preload
PTFE	No preload
PEEK	No preload

Table 3: Non-Metallic Materials Selected for Hydrogen Exposure

For elastomers, Halliburton standard micro dumbbells were prepared from the test slabs and loaded on the test sub. For engineered plastic, *ASTM D638 Type V* samples machined from the billets were used for exposure. Each sample were separated by spacers to avoid contact or sticking of samples while under exposure. No pre-stress was applied to the non-metallic sample while loading. Figure 6 illustrates the sample loading arrangement.

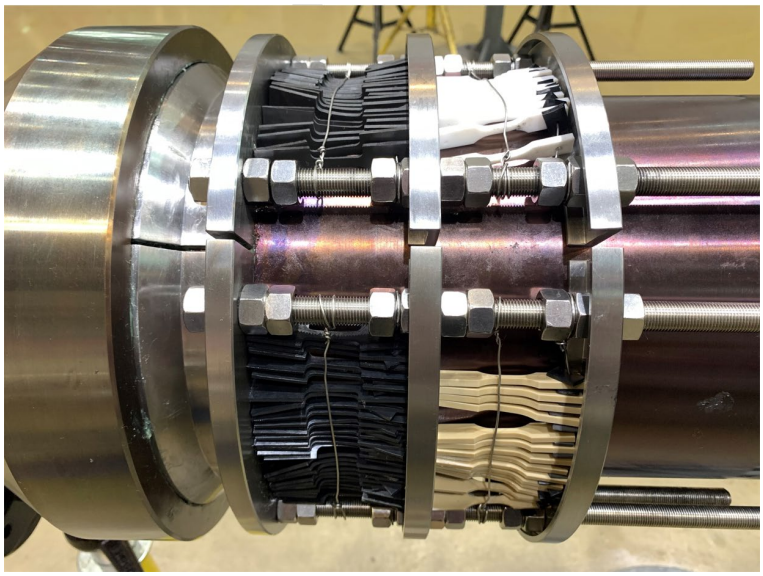

Figure 6: Non-Metallic Test Sample Loading Arrangement on Test Sub

“Exposed” in this context refers to the test coupons that were aged in high-pressure hydrogen. “Un-exposed” refers to a corresponding test coupon with the same heat number but was not exposed to the well.

6. Testing Protocol

Metallic test coupons retrieved from the well were analysed by LPI to examine potential macro cracks on the surface. Following this, confocal laser scanning microscopy was performed to detect micro cracks. Finally, selected specimens were subjected to μ X-ray computed tomography (μ X-ray CT) that can detect micro cracks both on the surface and non-destructively in the bulk.

Total hydrogen absorbed by the metal was determined by TDMS. This data is indicative in nature as the test coupons were not preserved after they were removed from the well. As a result, the possibility of some hydrogen having outgassed during transport etc., cannot be ignored.

After TDMS, a set of samples were fractured in a standard tensile test in air and SEM was performed to study the fracture faces. The objective was to assess potential effects of hydrogen exposure on failure mechanisms.

The primary focus of the study at this stage was metal because it is less complex to examine. As a result, while the preliminary NDT inspection included weldments and coatings, further characterization and testing was restricted to bulk metal.

Non-metallic samples after exposure were visually inspected for surface damage and any defects attributed to rapid gas decompression. Bulk integrity of the material was evaluated through X-ray CT scan. Mechanical properties of non-metallic materials were evaluated both at room temperature and elevated temperatures to understand the effects hydrogen exposure.

The samples were then evaluated through various analytical methods to understand the effects of hydrogen on the chemical composition and degradation of the materials. Various analytical techniques, such as Fourier transformation spectroscopy, differential scanning calorimetry, and thermogravimetry, were used for this purpose.

The following sections discuss the testing performed.

Visual Inspection

Both metallic and non-metallic samples were visually inspected for surface defects or other exposure-related issues after retrieval from the well.

Metallic test coupons from the well were analysed by LPI to examine potential macro cracks on the surface.

At the Material Science Laboratory, non-metallic samples were further inspected for surface defects through a microscope at 10X and 20X magnification. High-magnification cross-sectional examination was performed on the samples to identify potential RGD-related cracks or voids. Visual inspection was performed in accordance with *Halliburton Internal Procedure*.

Confocal Laser Scanning Microscopy

A confocal laser scanning microscope focuses only on a single focal plane and the unfocused plane is not visualized. In contrast, the conventional microscopes do not filter the signal from the unfocused plane of the sample, which results in saturated and blurry images, particularly when oxides, pits, or other defects are present on the surface. Laser scanning was performed to observe potential micro cracks that might have been formed due to the presence of hydrogen in the pre-strained specimens.

X-Ray Computed Tomography (X-Ray CT)

To examine metallic materials, ZEISS Xradia Versa μX-ray CT system was used with a voltage of 450 kV. Gauge sections of as-retrieved specimens were subjected to the X-ray beam. A series of 2D cross-section slices was produced after image reconstruction. Beam optics (e.g., scanning rate, X-ray energy, and X-ray spot size) were optimized to achieve an ultra-high resolution of ~8 μm. This is remarkable considering that typical resolutions achievable while analysing sizeable metal coupons is 5 to 100 μm. It required approximately five days of scanning and analysis time for each specimen to achieve such high-resolution data. The capability of the X-ray CT to resolve at such fine scales through the bulk of the metal establishes this technique as a unique non-destructive method to study hydrogen-induced cracking.

X-ray CT scanning helps identify possible bulk defects in polymeric materials. An X-ray CT scan was performed on the exposed and unexposed samples to identify imperfections in the polymer matrix as well as cracks at the polymer matrix and polymer-to-filler interface. Some published studies indicate the presence of micro cracks at the filler-to-polymer interface is attributed to hydrogen exposure. X-ray CT scanning was performed using SkyScan 2111 at 50KVsource voltage and at a magnification level of 1 micron for non-metallic materials.

Thermal Desorption Mass Spectroscopy (TDMS)

A Leco DH603 hydrogen analyser was used to determine the concentration of total hydrogen absorbed by metallic materials. The method involves placing a pre-weighed sample into a furnace and allowing the hydrogen to be evolved by hot extraction. A flowing stream of an inert gas is used to sweep the evolved hydrogen into a thermal conductivity detector, which measures the hydrogen content. If samples are preserved at a low enough temperature to suppress hydrogen from outgassing, this equipment can also be used to measure diffusible hydrogen. Hydrogen uptake was measured according to *Halliburton procedure.*

Tension Tests

A set of metallic specimens retrieved from the well were selected for standard tensile testing in air. A corresponding set of unexposed test coupons was also subjected to tensile testing. Both the exposed and unexposed test coupons fractured in tension were examined to study how hydrogen could have affected the failure process. Tensile testing was performed according to *Halliburton procedure.*

Tension testing of elastomeric materials was conducted on Halliburton micro-tensile samples in accordance with *internal specifications* at 10 in./min with three replicates. Halliburton evaluated the equivalence of the micro-tensile samples against the *ASTM D412* standard r. Tensile properties of the samples were tested according to *ASTM D638*. For PTFE materials, the strain rate used was 2 in./min and PEEK materials were tested at 0.2 in./min.

When possible, the median of the three replicate samples was used to establish changes in tension properties for tensile stress at break (σ_b), tensile strain at break (ε_b), and tensile modulus at 25% (M_{25}) and 50% strain (M_{50}).

For Non-Metallic materials, tension testing was performed at both room and elevated temperatures according to *Halliburton internal procedures.* Any micro defects attributed to hydrogen entrapment, such as cracks at the polymer matrix or the filler-to-polymer interface, can significantly impact tensile properties when tested at elevated temperatures. Any micro-structural defects will significantly change the elevated tensile properties.

Scanning Electron Microscopy (SEM)

Fracture faces of the exposed and unexposed metallic test coupons were analysed by a Joel 7600F field-emission SEM. This is a high-resolution electron microscope that can detect the signs of hydrogen related failure at a finer length scale. There is ample literature that details how SEM has been used to identify hydrogen-induced quasi-cleavage fracture and intergranular cracking in structural alloys. Consistent with this, SEM fractographs were collected from the exposed test coupons and compared to those of unexposed coupons to assess whether they exhibited discernible signs of hydrogen embrittlement.

Specific Gravity/Hardness

Specific gravity and hardness testing of elastomeric materials was performed on 1×1-in. specimens aged with two replicates. Changes in specific gravity and hardness can indicate swelling, chemical, or thermal degradation. Specific gravity was tested according to Halliburton internal procedures.

FTIR Evaluation

FTIR evaluation is a method typically used to identify unknown materials; it uses the absorption characteristics of chemical bonds to create a unique fingerprint of a material. The FTIR scan can typically be used to characterize different classes of materials but is more frequently compared to a library of known material scans. FTIR analysis was performed on a Thermo Scientific™ Nicolet™ iS50 spectrometer. FTIR scan peaks were generated from unexposed and exposed materials and compared. Any changes in the spectra—new peaks created on exposure or changes in the absorption levels of existing peaks—indicates possible chemical reactions experienced by the exposed samples. FTIR evaluation was conducted according to Halliburton Internal procedure.

Thermogravimetric Analysis (TGA)

TGA is an important tool used for material characterization. It is a technique in which the mass of the substance is monitored as a function of temperature and time in the controlled atmosphere, thus providing quantitative analysis of the substance. The standard test method for compositional analysis of polymer by TGA is based on determining the quantity of four defined components: highly volatile matter, matter of medium volatility, combustible material, and ash left after oxidative decomposition of inorganic components. Any changes in these components after exposure indicates chemical degradation or swelling of the material in the presence of the exposed medium. Table 4 defines the different fractions during TGA of elastomers.

Highly Volatile Matter	Moisture, polymer, diluent, plasticizer, cure accelerator, antioxidants, etc. (400°C (752°F) or lower)
Matter of Medium Volatility	Processing oil, processing aid, elastomer, resin, absorbed higher-molecular-weight oil components, etc.; in general, these materials degrade at >400°C (752°F)
Combustible Material	Oxidizable material, not volatile at 600°C (752°F) —carbon black, graphite
Ash/ Residue	Non-volatile residues in an oxidizing atmosphere, which can include metal oxides, filler, or inert reinforcing materials; a small amount of ash (<1%) could be attributed to elastomer residue

Table 4: Definitions of Different Fractions During TGA of Tested Rubber

Tests were conducted at a constant heating rate of 20°C/min (68°F/min) from room temperature to 1000°C (1832°F). For elastomers, the initial heating phase up to 600°C (1112°F) was conducted in a nitrogen environment and then up to 1000°C (1832°F) in the presence of oxygen. For engineer plastic, a heating cycle was performed in a nitrogen environment. Changes in composition percentage at each component level were calculated for the exposed materials compared to the unexposed material to understand the effects of exposure. TGA analysis was conducted according to Halliburton internal procedures. Differential Scanning Calorimetry (DSC) Analysis

DSC is a powerful tool used to measure the glass transition temperatures of elastomers and the melting and crystallization temperatures of plastic. These important properties assist polymer characterization. Glass transition temperature (Tg), melting temperature, and crystallization temperature (Tc) of the material are expected to change significantly if the sample experiences thermal or chemical degradation. Any chemical or thermal degradation of the material can impact the transition temperatures. The analysis was performed according to *Halliburton internal Procedure.*

7. Results

Metallic Materials

Effects of Hydrogen on Surface and in the Bulk

None of the metallic specimens listed in Table 2 exhibited any effects attributed to hydrogen exposure on the surface. LPI did not indicate any macro cracks. Confocal laser scanning microscopy revealed various degrees of pitting, possibly attributed to brine injection; however, micro cracks attributed to hydrogen embrittlement were not observed.

Figures 7 through 9 are representative laser scanning micrographs of a low-alloy steel (4140-125), martensitic stainless steel (410SS-80), and a Ni-base superalloy (alloy 925-110) test coupon. It was observed that, while pits occur over the entire surface of the 4140 specimens, the severity of pitting is significantly reduced for 410 SS. The surface of alloy 925 is nearly defect-free. Average pit depth is ~40 µm in 4140 and 16 to 20 µm in other grades.

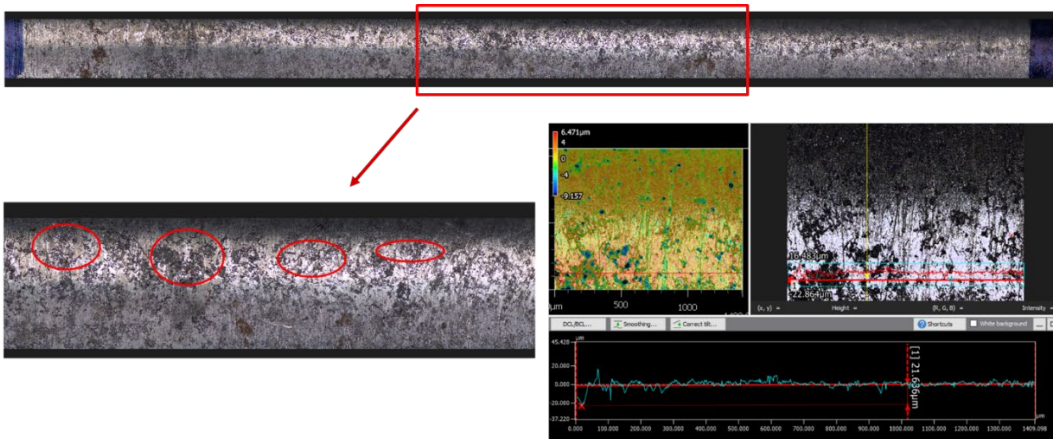

Figure 7: Laser Scanning Micrographs of a Low-Alloy Steel (4140-125) Test Coupon

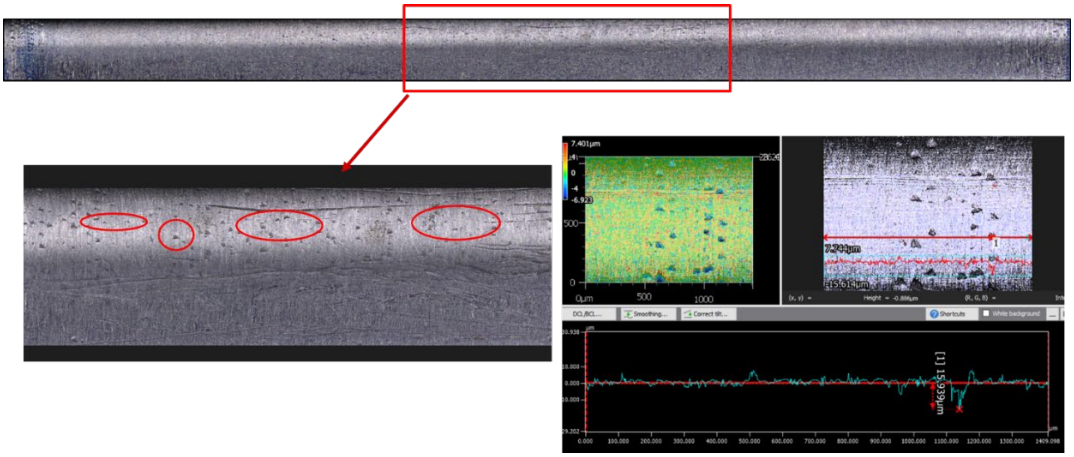

Figure 8: Laser Scanning Micrographs of a Martensitic Stainless Steel (410SS-80) Test Coupon

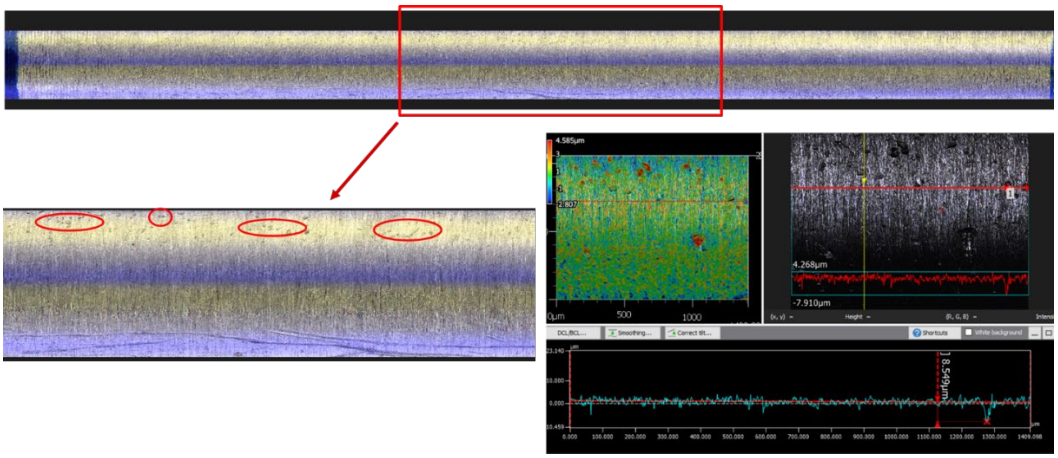

Figure 9: Laser Scanning Micrographs of a Superalloy (Alloy 925-110) Test Coupon

While laser scanning accurately detects surface irregularities, it cannot resolve defects in the subsurface or in the bulk of the metal. μ X-ray CT is more appropriate for such analysis. A select set of metal test coupons were analyzed by μ X-ray CT to examine through-thickness micro cracks caused by hydrogen exposure.

Figures 10 through 12 illustrate representative 2D slices reconstructed from μ X-ray CT data of a low-alloy steel (4140-125), martensitic stainless steel (410SS-80), and a Ni-base superalloy (alloy 925-110) test coupon.

X-rays were transmitted through the sample to hit the detector and create an image. Concurrently, the sample was rotated and approximately 5,000 2D projections were collected. The raw output was a series of projections of the sample collected at many different angles. These projections were digitally "reconstructed" using an inverse algorithm to view the sample as "slices" of 2D cross-sections shown in Figures 10 through 12.

No evidence of hydrogen-induced cracking was observed in any of the metal specimens listed in Table 2. The 4140-grade exhibited considerable pitting, while 925 and martensitic SS grades were less affected, which is consistent with the laser scanning data. Most of the subsurface and bulk was featureless and lacked any absorption contrast, revealing that the bulk of the metal remained intact without hydrogen-induced damage.

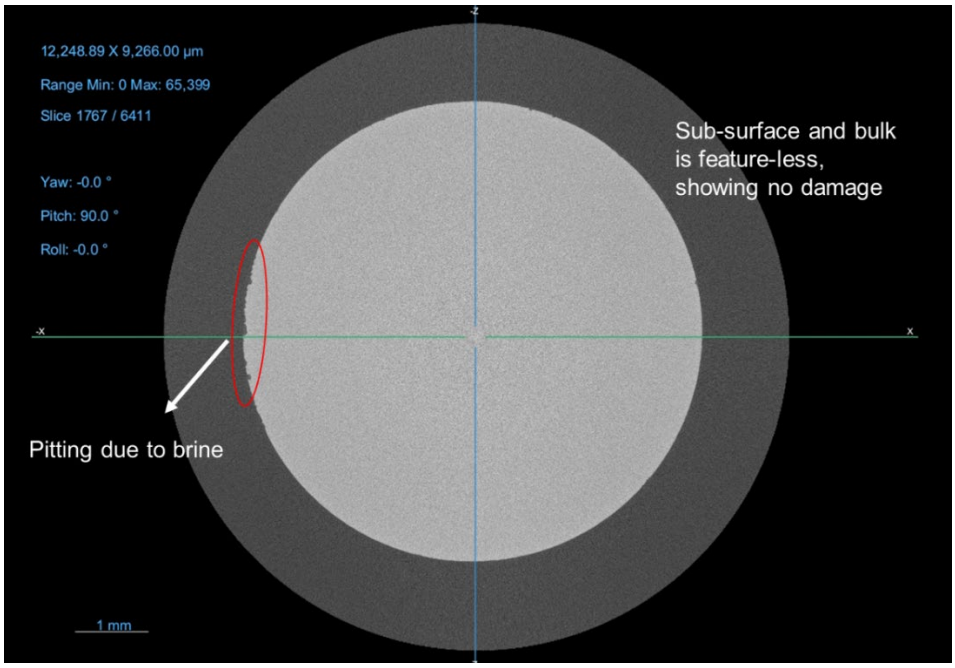

Figure 10: Representative 2D Slice Reconstructed from μ X-ray CT Data of 4140-125

These experiments show that X-ray CT can resolve features at ~10 μm length scales through the bulk of the metal coupons without damaging them or requiring any specific sample preparation. This makes it a unique non-destructive technique to study hydrogen-induced cracking.

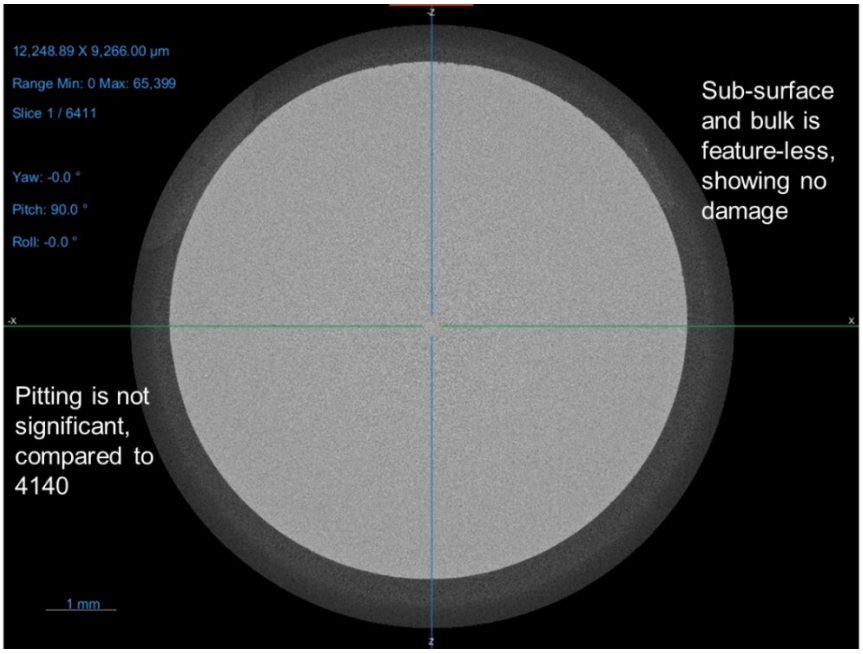

Figure 11: Representative 2D Slice Reconstructed from µ X-ray CT Data of 410 SS

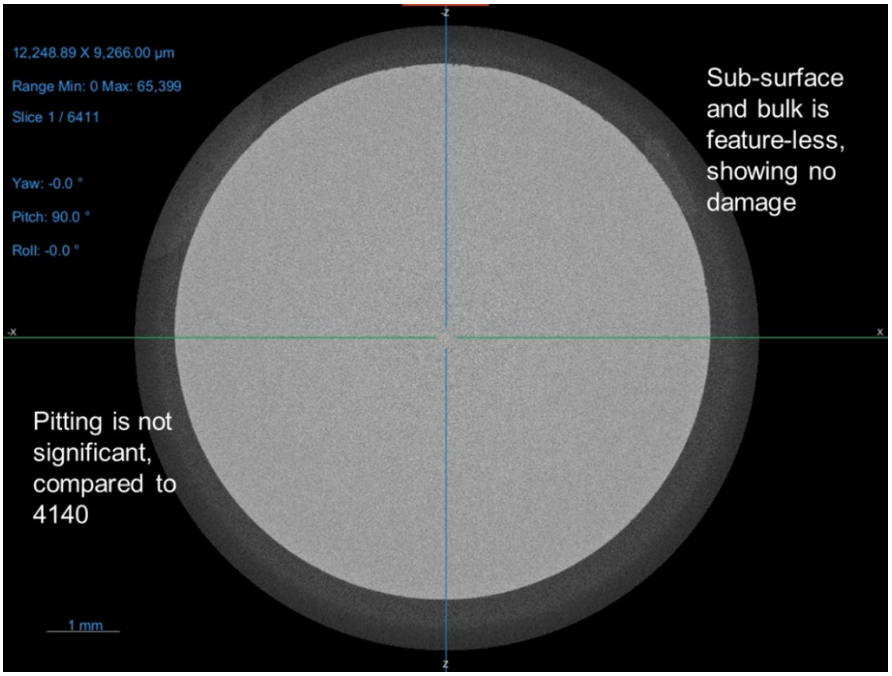

Figure 12: Representative 2D Slice Reconstructed from µ X-ray CT Data of Alloy 925

Hydrogen Uptake and Effects of Microstructure

Severity of hydrogen embrittlement is often correlated with hydrogen uptake. Hydrogen that is free to diffuse within the metal is termed diffusible hydrogen. Most of the hydrogen in ferritic metal is diffusible hydrogen. In contrast, metal with austenitic structures does not permit much diffusion; instead, it tends to trap hydrogen atoms. Total hydrogen uptake is the sum of diffusible and trapped hydrogen.

TDMS was performed to measure total hydrogen uptake in metal during well exposure. Measuring diffusible hydrogen requires the samples to be preserved at low temperatures to suppress hydrogen outgassing. Because this could not be performed due to practical limitations during sample transport from The Netherlands to Singapore, diffusible hydrogen was not measured for these samples.

Figure 9 shows total hydrogen uptake in selected low-alloy steel grades, martensitic stainless steel, and superalloy, along with the raw data (i.e., intensity vs. time). The area under this curve corresponds to the concentration of hydrogen in ppm. While this data is indicative in nature because the possibility of some hydrogen outgassing cannot be eliminated, the results shown in Figure 13 are still qualitatively meaningful and consistent with the literature.

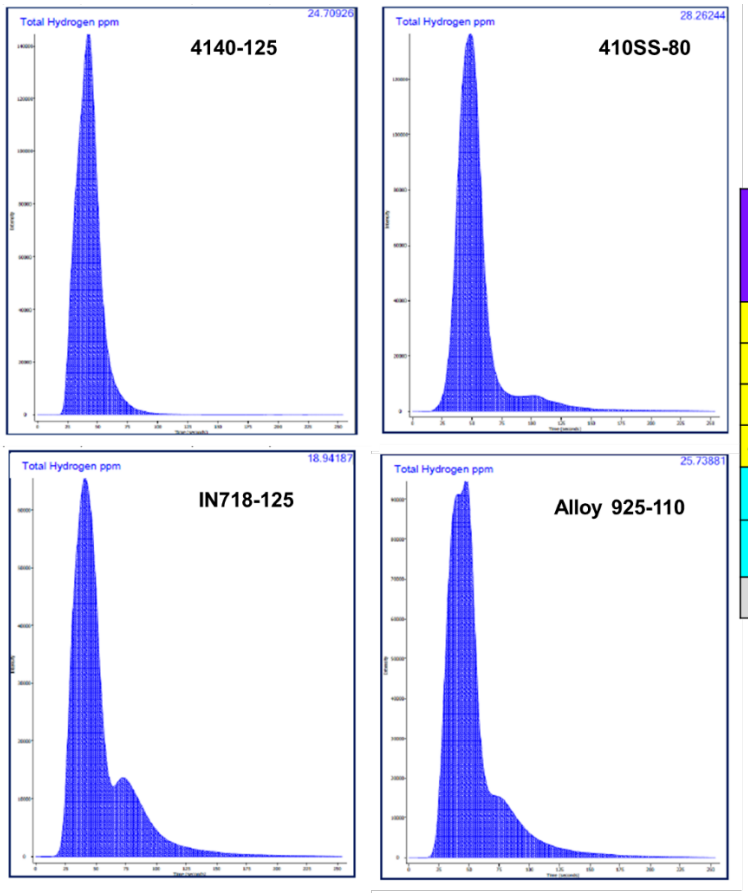

Alloy	Total [H] w-ppm
4140-125	0.44
4140-80	0.32
4130M-110	0.29
4130M-125	0.54
925-110	2.76
NI718-125	3.42
410SS-80	3.62

Figure 13: Hydrogen Uptake Data from TDMS

The concentration of total hydrogen varies between 0.29 and 0.44 w-ppm in low-alloy steel (41XX grades). This is smaller compared to the 2.76 to 3.42 w-ppm of hydrogen that was absorbed by the two Ni-base superalloys. Because of their ferritic microstructure, 41XX grades do not trap hydrogen. In contrast, superalloy, such as, IN718, has an austenitic structure and traps hydrogen. This explains the observed hydrogen concentrations in the two alloy systems.

The martensitic stainless-steel grade (410 SS) has a ferritic/distorted ferritic structure; so, in theory, it should not trap hydrogen and total hydrogen uptake should be comparable to 41XX grades. However, Figure 9 shows 3.62 w-ppm of hydrogen in 410SS, which is significantly higher compared to 41XX grades.

Literature as well as previous Halliburton research on martensitic stainless steel suggests high dislocation densities in martensitic stainless-steel grades because of its hierarchical microstructure. The abundance of interfaces, such as those at laths, blocks, packets, and dislocations, provide many local trapping sites that can bond with hydrogen. This explains the higher hydrogen uptake observed in the TDMS data.

Effects of Hydrogen on Failure Mechanisms

SEM fractography was performed to study potential changes in failure mechanisms attributed to hydrogen exposure. Because none of the metallic specimens retrieved from the well exhibited any

cracks, select low-alloy steel test coupons were subjected to tensile testing in air to create a fractured surface. A corresponding set of unexposed test coupons was also fractured in tension to establish a reference. Both the exposed and unexposed test coupons were examined by SEM.

Figure 14 shows SEM fractographs of the two 4140-125 test coupons—exposed and unexposed. “Exposed” here refers to the specimen that was aged in the pilot well. “Unexposed” refers to another test coupon from the same heat number that was not exposed. Fracture faces of 4140-125 show clear evidence for micro-void coalescence, both before and after well exposure. When hydrogen embrittlement effects are significant, ferritic steel exhibits intergranular and/or quasi-cleavage fractures. In this case, no evidence of such fractures was observed, which indicates that the failure mode remains ductile throughout.

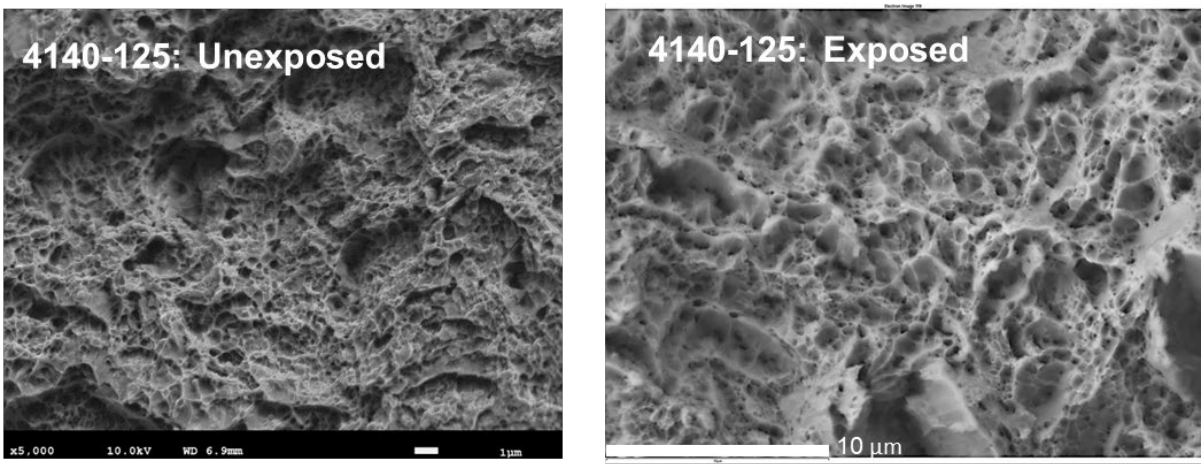

Figure 14: SEM Fractographs Of Two 4140-125 Test Coupons—Exposed to The Gasunie Well and Unexposed Showing Micro Voids

Figure 15 shows SEM fractographs of the exposed and unexposed test coupons on a coarser length scale, where the extent of shear lips is clearer. Consistent with Figure 12, it can be observed that a pronounced shear lip zone (shown by arrows) is present both before and after the well exposure. This provides additional evidence to suggest that the metal retains its capability to plastically deform, even after ageing in high-pressure hydrogen

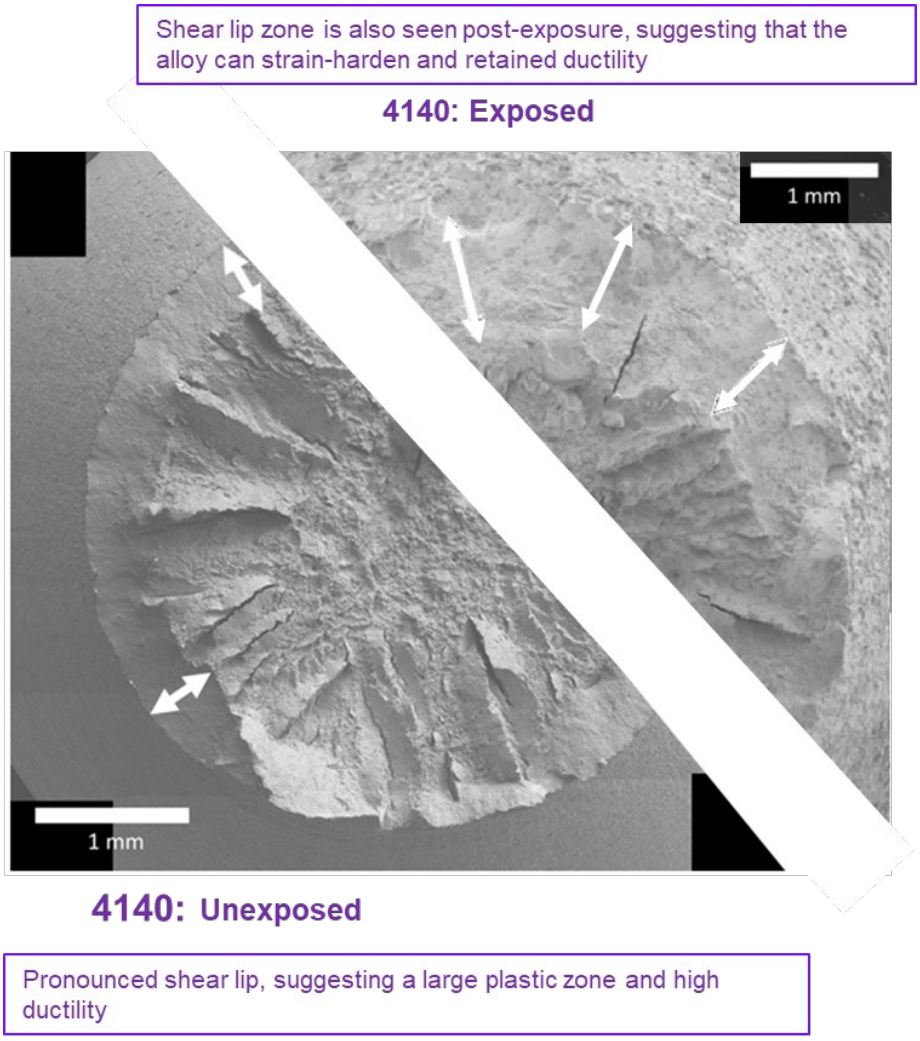

Figure 15: SEM Fractographs Of Two 4140-125 Test Coupons—Exposed to The Gasunie Well and Unexposed Showing Pronounced Shear Lip Zones

Non-Metallic Materials

Effects of Hydrogen on Visual and Bulk Properties

Visual inspection was performed on all the elastomers and engineered plastic exposed—HNBR, FKM, FEPM, FFKM, PTFE, and PEEK—and no surface defects, dents or bubbles, or signs of rapid gas decompression were observed on the samples. A high magnified inspection performed at 10X and 20X magnification on both elastomer and plastic samples was performed and no defects or micro cracks were observed on the samples. The filler dispersion on the elastomeric samples were observed unchanged compared to the unexposed samples.

X-ray CT was performed to identify bulk abnormalities on the polymer matrix. Some published literature has identified micro cracks at the polymer to filler interface of elastomeric materials while exposed to hydrogen. For all elastomers, no defects or cracks were observed on the bulk matrix. The polymer to filler interface was observed to be defect-free and the X-ray CT of the exposed samples was comparable to that of the original samples. The observations confirm the Halliburton recommendation that using rapid gas decompression elastomers with controlled bleed rates are suitable for hydrogen storage wells. Figures 16 through 23 present images of the visual inspection and Xray CT scans performed on various elastomers.

Bulk matrix of the engineered plastic tested—PTFE and PEEK—was also observed to be defect-free with no voids, cracks, or any other defects.

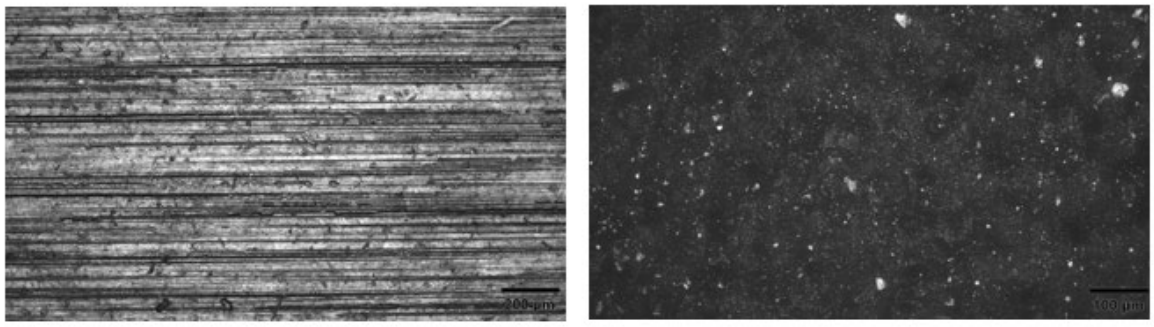

Surface Cross section

Figure 16: Microscopic Images of The HNBR Samples (20X Magnification) After Exposure; No Surface Cracks or Cross-Sectional Defects

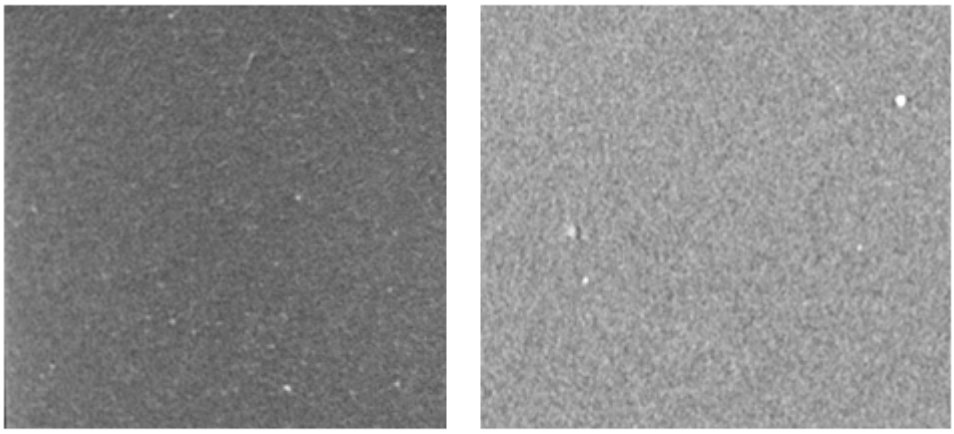

Unexposed Exposed

Figure 17: X-Ray CT Images of HNBR Before and After Exposure; Signs of Polymer-Filler Interface Cracks

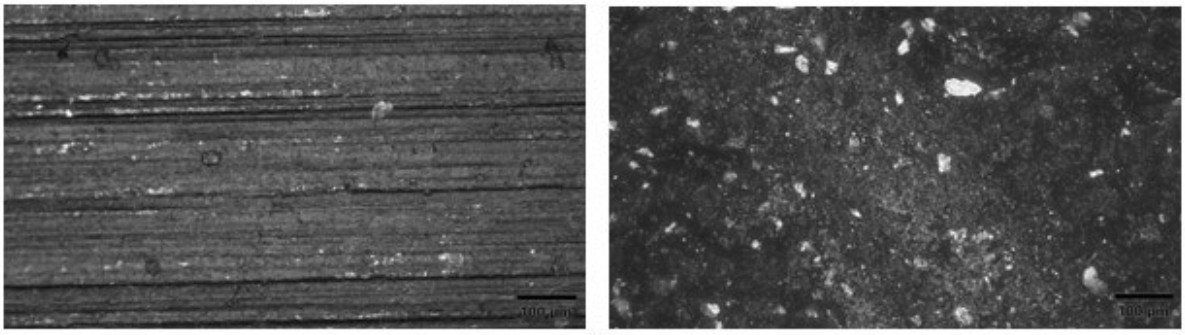

Surface Cross Section

Figure 18: Microscopic Images of The FKM Samples (20X Magnification) After Exposure; No Surface Cracks or Cross-Sectional Defects

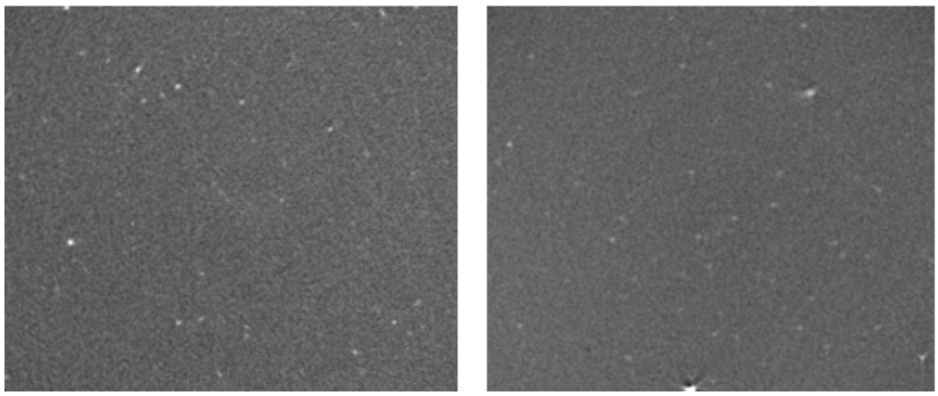

Unexposed Exposed

Figure 19: X-Ray CT Images of FKM Before and After Exposure; No Polymer-Filler Interface Cracks

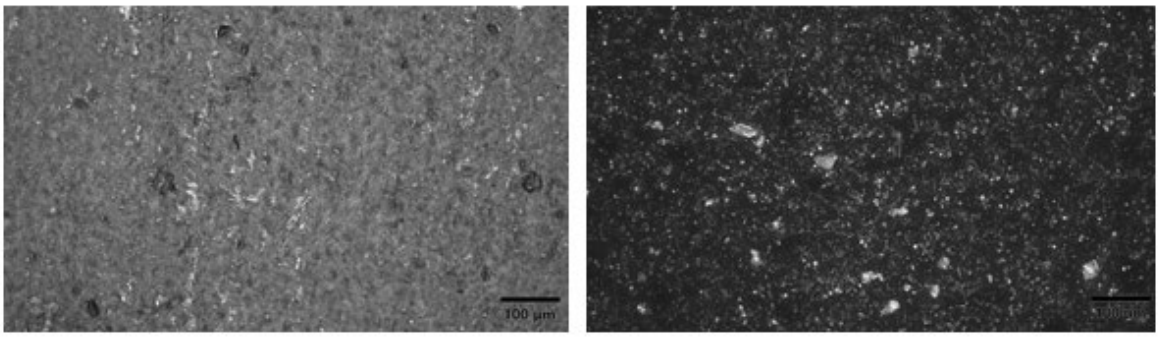

Surface Cross Section

Figure 20: Microscopic Images of The FEPM Samples (20X Magnification) After Exposure; No Surface Cracks or Cross-Sectional Defects

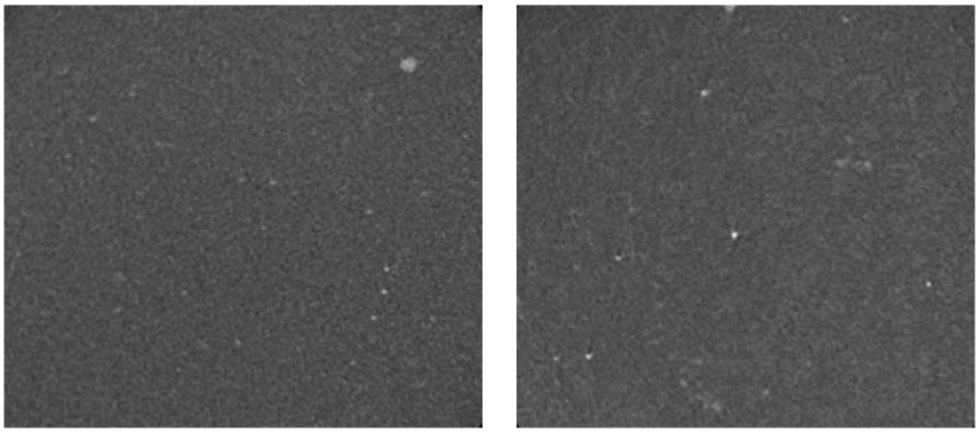

Unexposed Exposed

Figure 21: X-Ray CT Images of FEPM Before and After Exposure; No Polymer-Filler Interface Cracks

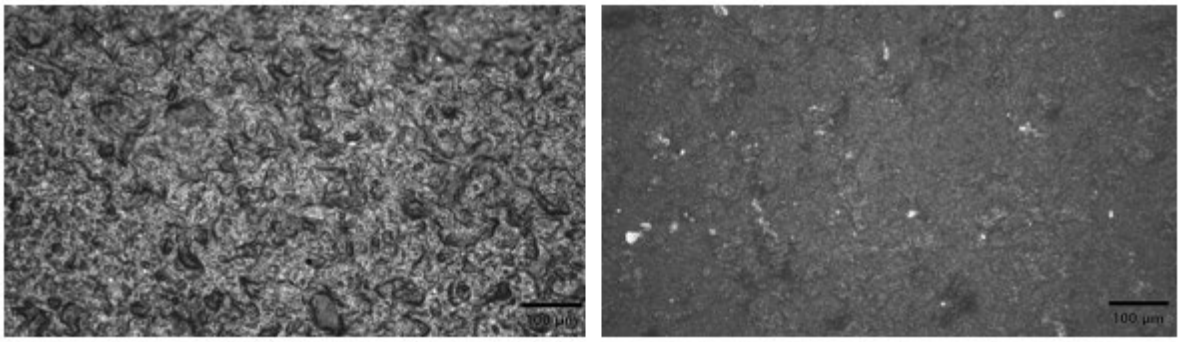

Figure 22: Microscopic Images of The FFKM Samples (20X Magnification) After Exposure; No Surface Cracks or Cross-Sectional Defects

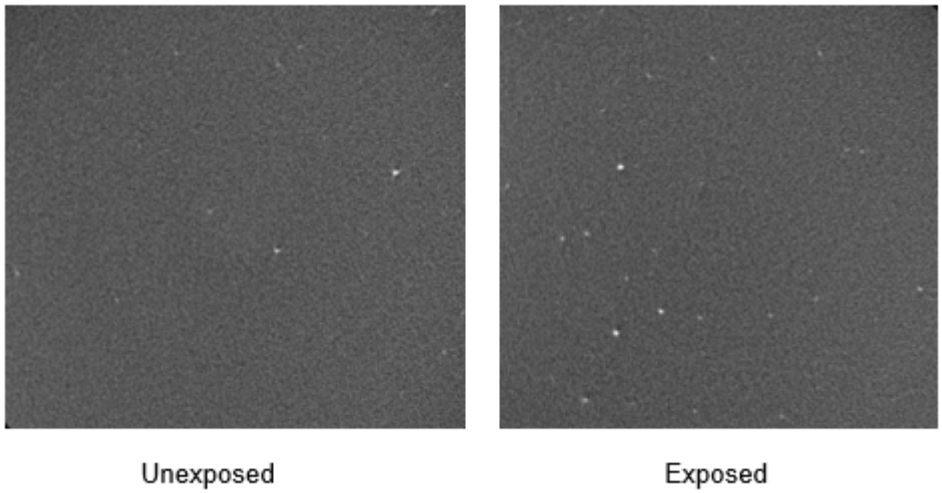

Figure 23: X-Ray CT Images of FKMM Before and After Exposure; No Polymer-Filler Interface Cracks

Effects of Hydrogen on Mechanical Properties

Hardness and specific gravity were tested on both elastomers and engineered plastic after exposure and compared to that of unexposed samples. Hardness and specific gravity changes provide indications of chemical degradation or swelling of the materials when exposed to hydrogen. The elastomers and engineered plastic were observed to be unaffected by hydrogen exposure.

Tensile properties of the exposed samples were evaluated both at room temperature 23°C (73°F) and elevated temperatures 149°C (300°F) and compared to the unexposed samples. Elevated temperature properties are helpful for aggravating the effects of bulk abnormalities and degradation, if any, in the exposed polymers.

Tensile properties of the exposed and unexposed HNBR samples exhibited no significant changes at room temperature. After exposure, ultimate tensile strength (UTS) changed by 2% with no change in elongation at break. No significant changes in the modulus data were observed at room temperature. At elevated temperature, UTS dropped by 26% and elongation at break by 11%. The change in 25% modulus was 22%. Changes in physical properties were well within the acceptance level for long-term exposure according to *ISO 23936-2* requirements. Based on the Halliburton performance rating table, HNBR compatibility rated “good.” High-temperature tensile data and the X-ray CT images confirmed the material did not experience any bulk defects.

No significant changes in FKM tensile properties were observed on hydrogen exposure. After exposure to hydrogen, the FKM material exhibited no change in UTS at room temperature. The elongation at break change at room temperature was 35% and modulus values at 25 and 50% elongation dropped by 27 and 25%, respectively. At elevated temperatures, the unexposed and exposed material tensile properties experienced a 14% decrease in UTS and a 15% increase in elongation. Modulus value of the exposed sample dropped by 29% compared to the unexposed samples.

FEPM polymers also exhibited no changes in properties when tested at both room and elevated temperatures. Changes in UTS, elongation at break, and modulus values were less than 10% between the exposed and unexposed samples, both at room and elevated temperature. No changes to specific gravity, hardness, or volume swell were observed between the exposed and unexposed samples. The compatibility of FEPM material is rated excellent according to the Halliburton rating system and is well within the acceptance limit of *ISO 23936-2* requirements for long-term use.

When tested at room temperature, the tensile strength of FFKM material decreased by 17% and the drop in elongation at break was 15%. Modulus at 25 and 50% elongation decreased by 12%, with no significant changes in hardness, specific gravity, or volume swell. Tensile properties at elevated temperature followed the same direction as the tensile strength and decreased by 30% with an elongation at break change of 17%.

The changes in tensile properties of elastomeric material exposed to hydrogen—HNBR, FKM, FEPM, and FFKM—were observed within the acceptance limit of *ISO23936-2* for long-term application and were within the acceptance limit provided by Halliburton internal protocol. No significant changes in PTFE tensile properties and no visual defects or surface cracks were observed during hydrogen exposure. Hardness and specific gravity of the material remained unchanged after exposure. UTS of hydrogen exposed PTFE material at room temperature testing changed by 9% and elongation at break decreased 19%. When tested at elevated temperature, the tensile and elongation at break change observed was 17 and 14%.

PEEK materials also did not exhibit any significant changes in properties when exposed to the hydrogen environment. Hardness and specific gravity of the material remained unchanged after exposure. UTS and yield strength changed by 20 and 14% from the unexposed samples, but the elongation values at break and yield revealed no significant changes. Elevated temperature, tensile, and elongation property changes were less than 5% in both break and yield cases.

The tensile property changes of both engineered plastic materials—PTFE and PEEK—were within the acceptance limit of *ISO23936-1* for long-term aging and met the Halliburton internal acceptance criteria for long-term use

Effects of Hydrogen on Chemical and Compositional Properties

Exposed samples were analysed for chemical property changes, including functional group analysis through FTIR, composition analysis through TGA, and transition temperature identification through DSC, to understand the effects of hydrogen on the chemistry of the polymer compound. Change in analytical properties are good indicators of polymer degradation.

Elastomers and engineering plastic exposed did not show any significant changes analytical properties. FTIR data from the exposed samples revealed to be excellent match with the unexposed samples. No significant changes in absorption were observed between peaks, and no new peaks were observed on the spectra. FTIR spectra for the non-metallic material exposed in comparison with the reference sample illustrated in Figure 24 through 29.

No significant changes in transition temperature measured using DSC and composition analysed through TGA observed for the exposed sample compared with unexposed samples. The analytical data results ruled out the possibility of chemical degradation and permanent swelling of the non-metallic material exposed. Summary of changes in transition temperature and composition is given in table 6.

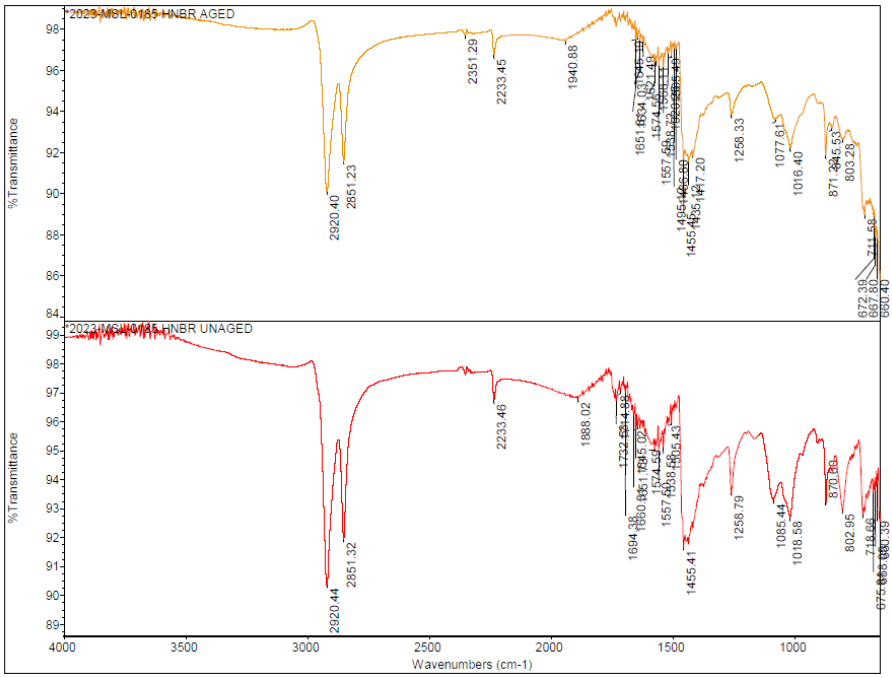

Figure 24: FTIR Scan from Both Unexposed (Unaged) And Exposed (Aged) HNBR Samples

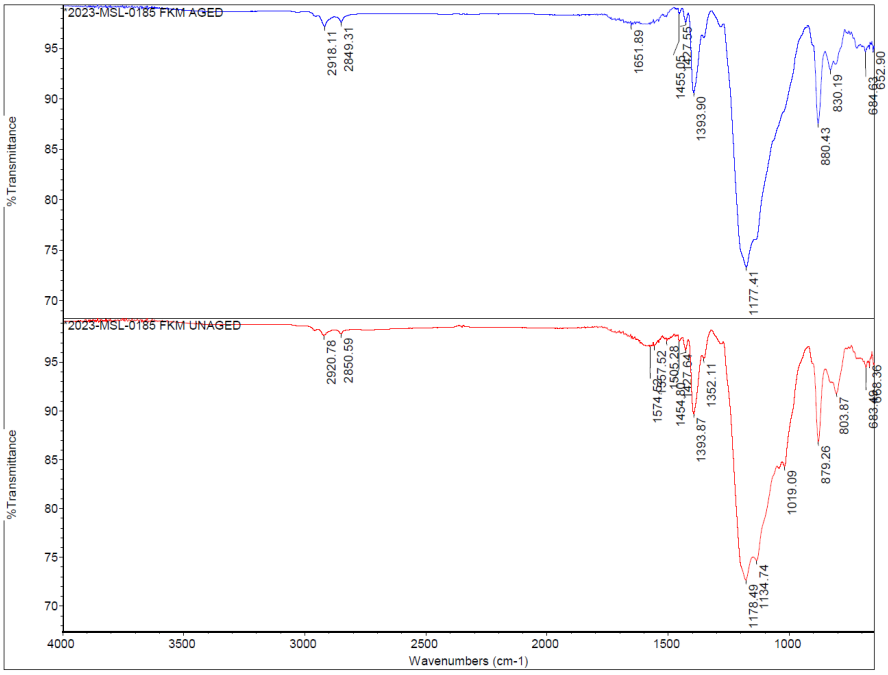

Figure 25: FTIR Scan from Both Unexposed (Unaged) And Exposed (Aged) FKM Samples

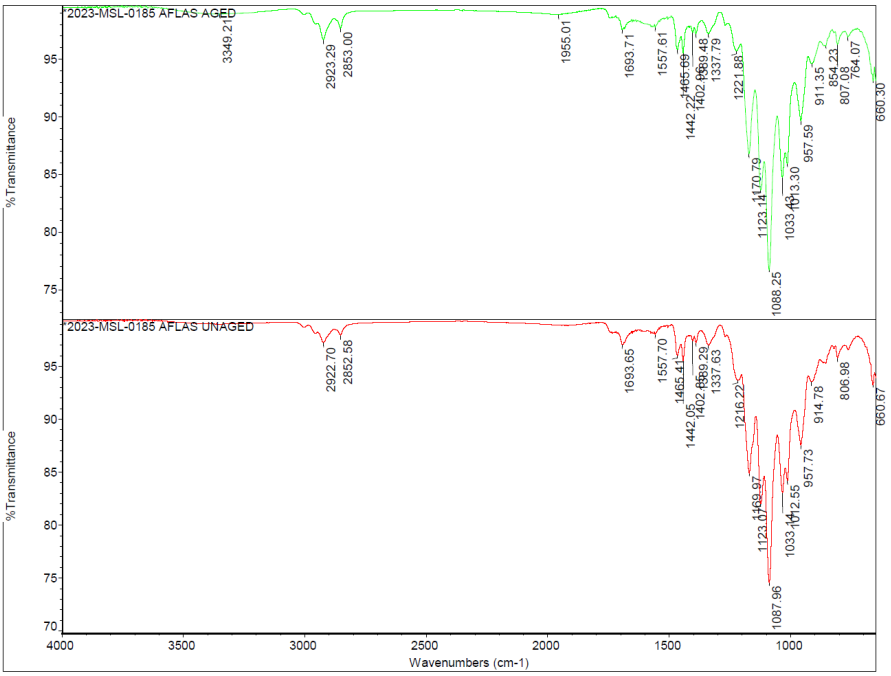

Figure 26: FTIR Scan from Both Unexposed (Unaged) And Exposed (Aged) FEPM Samples

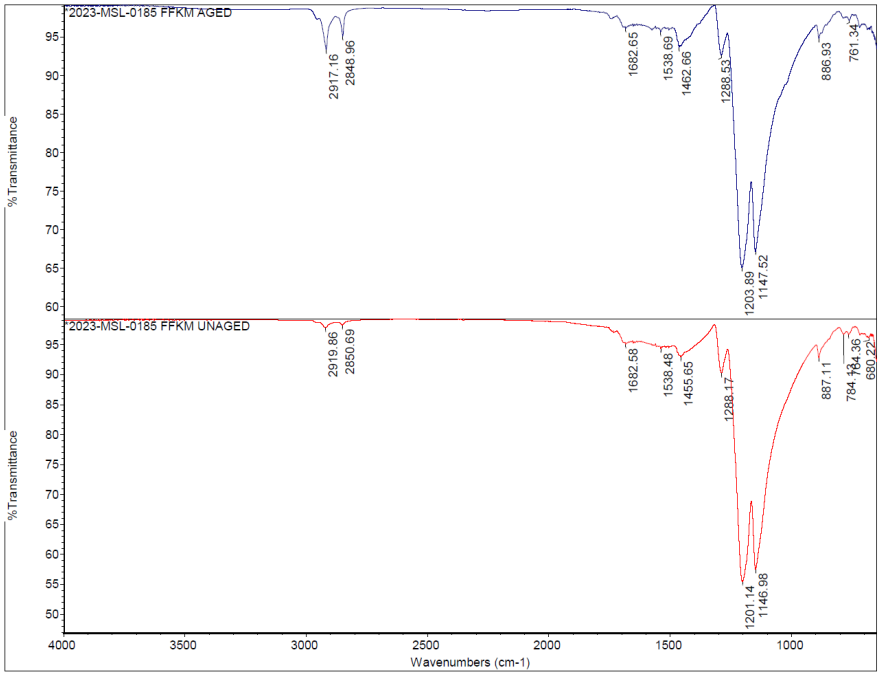

Figure 27: FTIR Scan from Both Unexposed (Unaged) And Exposed (Aged) FFKM Samples

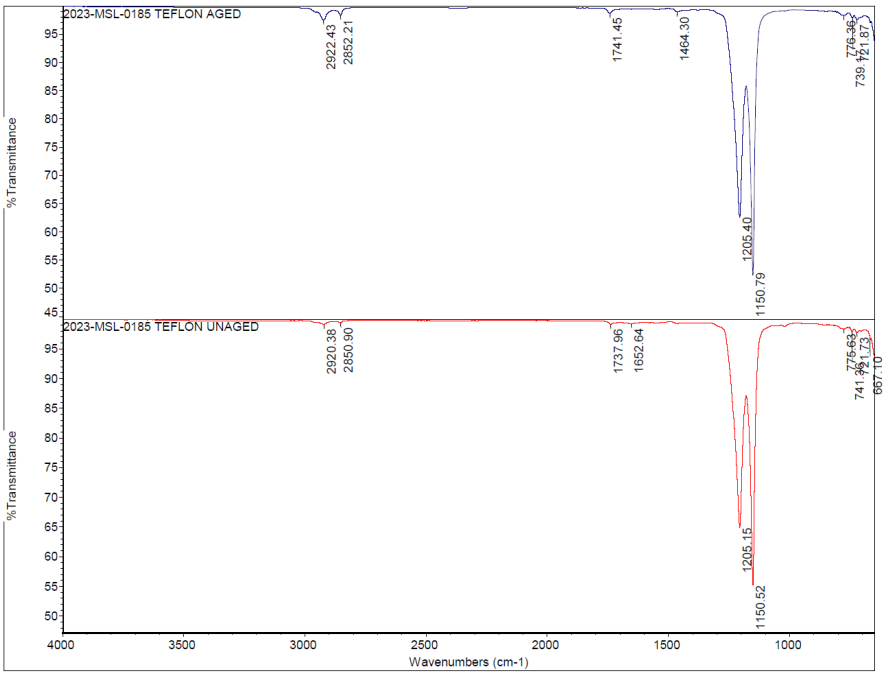

Figure 28: FTIR Scan from Both Unexposed (Unaged) And Exposed (Aged) PTFE Samples

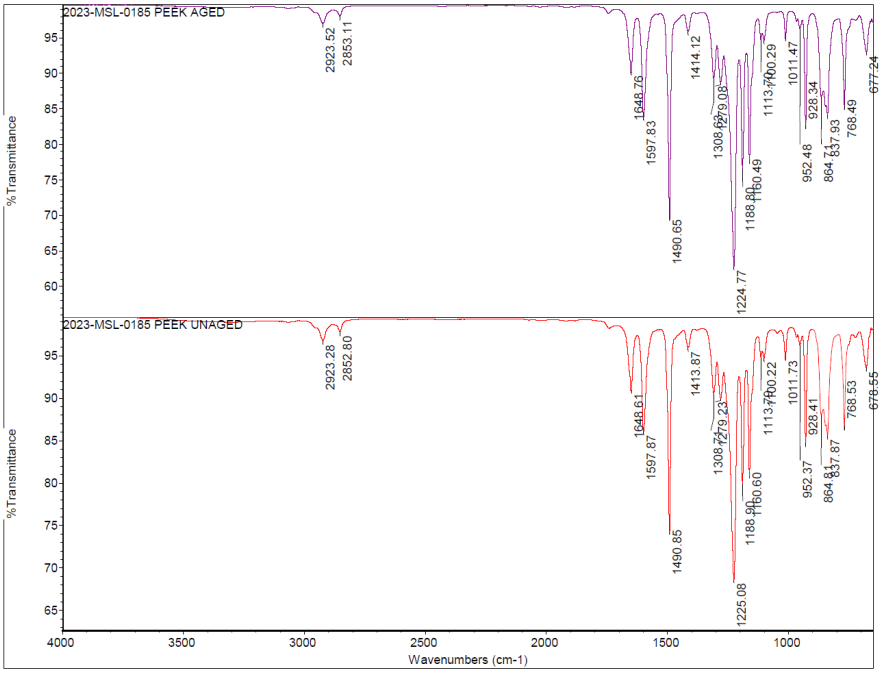

Figure 29: FTIR Scan from Both Unexposed (Unaged) And Exposed (Aged) PEEK Samples

Material Type	Changes in Transition Temp, °C	Changes in Composition			
		Highly volatile matter up to 400°C, %	Medium volatility 400 to 600°C, %	Combustible material 600 to 800°C, %	Residue at 800°C, %
HNBR	-2.20	1.24	-0.04	-1.47	0.27
FKM	-0.62	0.91	-2.82	2.03	-0.12
FEPM	-0.77	0.40	-0.29	-0.14	0.00
FFKM	-0.25	-0.02	0.58	0.44	0.00
PTFE	0.40	0.01	-0.19		0.31
PEEK	-0.29	-0.05	0.43		-0.39

Table 5: Changes In Transition Temperature and Composition of Non-Metallic Material Exposed to Pilot Well

8. CONCLUSIONS

Metallic Materials

Performance is reviewed of select low-alloy steel grades, Ni-base superalloy, and weldments and coatings subjected to stress at a range of 67 to 90% YS in a high-pressure hydrogen environment.

Metal types retrieved from the well were characterized by a variety of techniques to examine the presence of macro and micro cracks—both on the surface and in bulk. Total hydrogen uptake was determined by thermal desorption mass spectroscopy (TDMS).

Subsequently, selected samples were subjected to tensile tests and scanning electron microscopy (SEM) was performed to examine the fracture faces. While preliminary NDT inspection included weldments and coatings, further characterization focused on bulk metal. The results of the analysis are summarized as follows.

None of the specimens exhibited any discernible damage after removal from the fixture. No macro cracks were observed upon liquid penetrant inspection (LPI).

Finer micro-scale surface analysis of bulk metal specimens was performed using confocal laser scanning microscopy. No evidence was observed to suggest any hydrogen-induced crack formation on the surface.

μX-ray CT was performed to characterize subsurface and bulk. Consistent with laser scans, it confirmed the absence of hydrogen-induced surface cracks. Various degrees of pitting were observed, possibly attributed to brine injection before and after hydrogen injection. No defects were observed in the subsurface and the bulk of the metal was intact and damage-free.

TDMS data exhibited significantly lower hydrogen uptake in low-alloy steel compared to superalloy and martensitic SS grades. Low-alloy steel, because of its ferritic microstructure, does not trap hydrogen. In contrast, superalloy, such as, IN718 has an austenitic structure and traps hydrogen. Martensitic SS grades, despite their ferritic/ distorted ferritic structure, still trap hydrogen because of their high dislocation densities. These results are therefore as expected and consistent with the literature.

Fractography of low-alloy steel test coupons after tensile tests exhibited no change in fracture mode. Both before and after exposure, the metal exhibited predominantly micro-void coalescence on the fracture faces, which indicated the failure mode remains ductile even after exposure to high-pressure hydrogen.

Insights from this project suggest that the post-exposure test data from pilot wells results from a combined effect of several different loading conditions and chemistries that the material sustains during ageing. The current laboratory test protocols do not simulate such environments and stress profiles, making it difficult to establish a definitive correlation between material properties and the field

performance. Building up on the learnings from this project, Halliburton is performing further studies to identify representative chemistries and loading mode effects that control the hydrogen embrittlement behaviour of metals. The selected load profiles and environments that are likely to be significant – such as, strain rate, dynamic loading, hydrogen blended with humidity/ oxygen – are being incorporated in constant-K and fixed-K fracture toughness tests to guide the design and fitness assessment of downhole tools for hydrogen service environments.

Non-Metallic Materials

Four elastomer types—HNBR, FKM, FEPM, and FFKM—and two engineered plastics—PTFE and PEEK—were introduced to the hydrogen well. The following conclusions are based on various tests performed on the retrieved samples.

All exposed samples were received in good condition. No visual defects, surface damage, or RGD-related defects were observed on the sample surfaces. Microscopic and cross-sectional examination of the samples also confirmed no RGD-related defects.

HNBR, FKM, and FFKM samples exhibited some changes in tensile properties at both room and elevated temperatures. Tensile property changes were less than 35% and well within the acceptance limit of ISO 23936-2 and Halliburton Test Protocol D00327493 for long-term use. FEPM exhibited no significant changes in tensile properties at both room and elevated temperatures. Hardness and specific gravity of all elastomers exhibited no significant effects on aging.

PTFE and PEEK samples exhibited no significant changes in tensile properties after exposure. Property changes observed were within the 20% acceptance limit of ISO 23936-1 and Halliburton Internal test protocol for long-term use. No significant changes were observed in terms of hardness and specific gravity.

FTIR analysis performed on the exposed samples revealed no significant changes in the spectra. No new peaks developed and no changes in the absorbance percentages of the spectra were observed when the exposed and unexposed spectra were compared. The results confirm no chemical or thermal reaction; thus, no crosslinking, chain breakage, or formation of a new functional group occurred.

Differential scanning calorimetry (DSC) performed on the material under evaluation revealed no significant changes to transition temperatures, such as crystallization, glass transition, and melting temperature. The glass transition temperature of the HNBR, FKM, FEPM, and FFKM elastomeric samples after exposure revealed no significant changes from the original, which indicated no thermal or chemical degradation. The PTFE and PEEK thermoplastic materials also exhibited no significant changes in terms of crystallization, glass transition, and melting temperature.

Comparison of hydrogen-exposed samples to unexposed samples revealed no significant changes in composition; thus, no swelling attributed to the absorbance of low volatile components and no thermal or chemical degradation of the material occurred.

A micro-CT scan of the exposed polymer samples revealed no cracks, micro cracks, splits in polymer matrix, or cracks at the filler-to-polymer interface. The clean CT scan confirmed the RGD-grade materials performed well, as expected, followed by the bleed-off procedure.

Acknowledgements

The authors thank management of Halliburton and Nederlandse Gasunie N.V for research, resource and for granting permission to publish this work. Authors thank the following Halliburton Material Science Center of Excellence in Singapore team, including Siti Nurhanis Omar, Vishal Raut, and Mohamad Saifullrizan Abdul Rahman, Uma Mageswari for providing supplemental testing support and analysis. Authors also expresses the thanks to Prof. Upadrasta Ramamurty, Nanyang Technological University, Singapore for their technical guidance and support on testing.

References

1. Ali Haratian, Soroosh Emami Meybodi, Mohsen Dehvedar - A comprehensive review on the feasibility of large-scale underground Hydrogen storage in geological structures with concentration on salt caverns.
2. Aleksandra Małachowska, Natalia Łukasik, Joanna Mioduska and Jacek Gębicki - Hydrogen Storage in Geological Formations—The Potential of Salt Caverns
3. Jay Evans, Global Gas Group LLC and Tom Shaw, LK Energy LLC - Storage of hydrogen in solution mined salt caverns for long duration energy storage.
4. Alessandro Campari, Federico Ustolin, Antonio Alvaro, Nicola Paltrinieri - A review on hydrogen embrittlement and risk-based inspection of hydrogen technologies
5. Karthik Krishnan, Shashwat Shukla, Arpana Verma - Evaluation of Hydrogen Embrittlement Resistance of 41XX Cr-Mo Steels, 13Cr Stainless Steel in High Pressure Hydrogen Environment - AMPP Annual Conference March 2023.
6. Lütfi Ekmekci, Merlin Seifert, Clara Herrera -Susceptibility of Martensitic Stainless Steels to Hydrogen Embrittlement -AMPP Annual Conference March 2023.
7. Simmons K.L., Kuang, W., Menon, N. et al. 2018. Compatibility of Polymeric Materials Used in the Hydrogen Infrastructure. DOE Hydrogen and Fuel Cells Program.
8. A Review on Applicability, Limitations, and Improvements of Polymeric Materials in High-Pressure Hydrogen Gas Atmospheres - Winoj Balasooriya, Clara Clute, Bernd Schrittesser & Gerald Pinter
9. Compatibility of hydrogen with different materials - European Hydrogen Train the Trainer Programme for Responders.
10. Sandeep Thatathil - Performance Evaluation of Non-Metallic Materials in Hydrogen Storage Pilot Well – AMI conference 2023 - Polymers in Hydrogen and CCUS Infrastructure
11. ASTM A370-24a, Standard Test Methods and Definitions for Mechanical Testing of Steel Products. 2024 ASTM International.
12. ASTM E1316-22a, Standard Terminology for Non-destructive Examinations. 2023. ASTM International.
13. ASTM D412-16, International. Standard Test Methods for Vulcanized Rubber and Thermoplastic Elastomers—Tension. 2021. ASTM International.
14. ASTM D638-14, Standard Test Method for Tensile Properties of Plastics, 2022. ASTM International.
15. ASTM E1252-98, General Techniques for Obtaining Infrared Spectra for Qualitative Analysis. 2021. ASTM International.
16. ASTM D2240-15, Standard Method for Rubber Property—Durometer Hardness. 2021. ASTM International.
17. ASTM E1131-20, Standard Test Method for Compositional Analysis by Thermogravimetry. 2020. ASTM International.
18. ASTM D471-16a, Standard Test Method for Rubber Property—Effect of Liquids. 2021. ASTM International.
19. ASTM D3418-21, Standard Test Method for Transition Temperatures and Enthalpies of Fusion and Crystallization of Polymers by Differential Scanning Calorimetry. 2021. ASTM International.
20. C. Busollo, E. Abdo, E. Baronio, C. Starinieri, Qualification of Downhole Safety Valves for Use in Underground Hydrogen Storage Wells, SPE-220065-MS, 2024
21. API 14A 13th Edition. Subsurface Safety Valve and Annular Safety Equipment. 2024. American Petroleum Institute.
22. API 11D1 4th Edition. Packers and Bridge Plugs. 2021. American Petroleum Institute.
23. API 14B 6th Edition. Design, Installation, Operation, Test, and Redress of Subsurface Safety Valve Systems. 2015. American Petroleum Institute.